Positron scattering from polar molecules: Rotovibrationally inelastic collisions with CO targets

F. A. Gianturco,* T. Mukherjee,† and P. Paioletti
Department of Chemistry, The University of Rome, Città Universitaria, 00185 Rome, Italy
(Received 21 February 1997)

Quantum calculations have been carried out on the vibrational and rotational excitation processes for CO molecules in collision with positron projectiles below the threshold of Ps formation ($E_{\text{coll}} \leqslant 7$ eV). The coupled equations have been solved for the vibrationally inelastic process in the body-fixed frame of reference, and Born-type corrections for the divergent behavior of the angular distributions due to the permanent molecular dipole have been applied. Detailed comparisons are made between the partial (rotational and/or vibrational) integral and differential cross sections and earlier available calculations and measurements.
[S1050-2947(97)09309-8]

PACS number(s): 34.50.Gb, 34.80.Bm

I. INTRODUCTION

Unlike low-energy electron-molecule scattering processes, where the collision dynamics for the simpler diatomic targets is now well documented both experimentally and theoretically [1,2], the detailed behavior and the physical interpretation of low-energy positron (e^+) scattering from the same molecular targets are still not fully understood. Although the absence of exchange-correlation effects should make the theoretical modeling somewhat simpler, the delicate nature of the polarization effects and the occurrence of positronium (Ps) formation (either real or virtual) still make the corresponding calculations difficult to carry out. It is only recently that positrons have become a valuable tool for probing a wide range of phenomena in chemistry and molecular science [3–5], and the issue of positron attachment to atoms and molecules has become crucial to the interpretation of such studies.

The fact that the observed enhancement in positron annihilation rates [6] could proceed via a number of competing processes (e.g., bound-state formation in the e^+-molecule system, bound states of the Ps-molecule complex, excitation of molecular degrees of freedom, etc.) makes it essential to perform as many *ab initio* calculations as possible for the relevant e^+-molecule systems, while rather few of them are available even for the simplest molecular targets [7,8]. We recently began to carry out calculations for vibrating molecular targets which make use of a parameter-free formulation of the full positron-molecule interaction, and looked into the effects that the coupling of positron motion with molecular vibrations has on the final cross sections [9,10]. The present study is an extension of such an analysis to a rotating-vibrating target which is also a polar molecule, a feature which adds considerable complications to the dynamics of electron-positron low-energy scattering calculations [11,12].

The system which we discuss here is the CO molecule in its ground electronic state ($^1\Sigma$). The scattering of positrons from this polar target was experimentally studied earlier by Kwan [13] and by Sueoka and Mori [14] who, however, presented only total integral cross sections without either resolving inelastic contributions or obtaining angular distributions at the same energies. Corresponding theoretical work has also been rather scarce: some earlier calculations by Jain [15] using a model polarization potential were followed by the R-matrix calculations of Tennyson and Morgan [16], who found rather different results from the previous ones. More extensive calculations that included differential cross sections (DCS's), momentum-transfer cross sections, and rotationally inelastic cross sections were given in a more recent study by Jain, where a different correlation-polarization potential was employed [17,18]. No reference to vibrationally inelastic collisions was made in the above work, while that problem was explicitly treated in a later study of long-lived resonances in e^+-CO scattering [18].

In the present work we intend to approach all the above aspects of low-energy positron scattering from CO targets (i.e., elastic scattering, angular distributions, and rotational and vibrational inelastic scattering long-lived resonances) from a general point of view by using a nonempirical interaction potential and by solving the vibrational close-coupled equations. Section II therefore discusses the details of the interaction and the corresponding quantum scattering equations for a nonrotating, nonvibrating molecular target which can yield integral elastic (rotationally summed) fixed-nuclei (FNA) cross sections. The treatment of vibrational degrees of freedom in a close-coupling, body-fixed (BF) formulation is further discussed in Sec. III, where our present results for the coupling potentials are also presented. Section IV further analyzes angular distributions and discusses the correction needed to remove the pathological behaviour of BF-FNA DCS's in the forward-scattering region [12,19]. Rotationally inelastic cross sections are presented and discussed in Sec. V, while Sec. VI gives our general conclusions.

II. INTERACTION AND DYNAMICS

Asymptotically, for a general, nonlinear e^+-molecule collision system, the polarization potential is given by

*Author to whom correspondence should be addressed. Present address: Dipartimento di Chimica, Città Universitaria, 00185 Rome, Italy. FAX: +39-6-49913305.
Electronic address: FAGIANT@CASPUR.IT
†Permanent address: Department of Theoretical Physics, Indian Association for the Cultivation of Science, Jadavpur, Calcutta 32, India.

$$V_{\rm pol}(r,\theta,\phi)=\frac{-1}{2r^4}\,[\,\alpha_0(4\pi)^{1/2}S_0^{01}+\alpha_2(\tfrac{4}{5}\pi)^{1/2}S_2^{01}+\alpha_1^2(\tfrac{4}{15}\pi)^{1/2}S_2^{21}], \quad (1)$$

where S_l^{mq} is a real spherical harmonic [20], (r,θ,ϕ) are the coordinates of the projectile referring to the center of mass (c.o.m.) of the target, and the spherical (α_0) and nonspherical (α_2 and α_2^1) polarizabilities are expressed in terms of the polarizability tensor α_{ii} of the target, namely,

$$\alpha_0=\tfrac{1}{3}(\alpha_{11}+\alpha_{22}+\alpha_{33});\alpha_2=\tfrac{2}{3}(\alpha_{33}-\tfrac{1}{2}\alpha_{11}-\tfrac{1}{2}\alpha_{22}),$$

$$\alpha_2^1=\alpha_{11}-\alpha_{22}. \quad (2)$$

The above asymptotic form [Eq. (1)] of the polarization potential is not true when the projectile is near the target. A simple remedy has been to multiply Eq. (1) by a cutoff function involving some adjustable parameter; nevertheless, this approach is unsatisfactory, although the results may be ''tuned'' to agree with observations (see, for example, Ref. [21]). For e^+ collisions, most of the calculations prior to 1984 used an electron polarization potential (EPP), assuming that such distortion effects are not sensitive to the sign of the charge of projectile. Morrison and his group [22] found that there is a need to generate a true positron polarization potential (PPP) rather than employing the EPP: they strengthened their point by presenting detailed calculations on the e^+-H_2 and -N_2 systems and comparing them with experimental data. Although earlier calculations on the e^+ collisions using the EPP gave good results as compared to experimental total cross section (σ_t) values, these theoretical results are generally poor at low energies. The more rigorous calculations, based on the variational polarized-orbital theories, are not satisfactory either; Elza *et al.* [22], for instance, had to introduce a cutoff function in both the short- and long-range interactions, and adjust two parameters to bring theory and measurement into close agreement. Even in a more sophisticated R-matrix approach, an accurate inclusion of polarization effects has not yet been realized [23].

Here we summarize a computationally simple form of the e^+-polarization potential which is different from the corresponding EPP, and does not contain any arbitrary parameter which can be externally adjusted to fit some preselected experimental features. The basic philosophy of the present approach is similar to the method of O'Connel and Lane [24] for the case of e^- scattering based on the correlation energy of the target in the presence of an incoming electron. Very recently, we modified the density functional approach method for the e^+ case by removing the exchange energy from the problem [25], and found this approach to be better than the EPP model, and closer to a more realistic PPP model. The present PPP is also based on the correlation energy of a localized e^+ in an e^- gas, and its hybridization with the correct asymptotic form [Eq. (1)]. The incoming e^+ is assumed to be a charged impurity at a fixed distance in an homogeneous e^- gas.

Arponen and Pajanne [26], in fact, applied a different approach to the problem of a light impurity in an electron gas. In their method the electron gas is described by a set of interacting bosons representing the collective excitations in the random-phase-approximation. Further, Boronski and Nieminen [27] described the density-functional theory of the electron-positron system, and presented the results on the positron-electron correlation energy as a function of the density parameter $\mathbf{r}_s$ (see below) for different $n_+(\mathbf{r})/n_-(\mathbf{r})$ ratios including the case of one positron in a homogeneous electron gas. Here n_+ and n_- denote the densities of positrons and electrons, respectively.

Based on the above work, explicit expressions for the e^+-e^- correlation energy $\epsilon_{\rm corr}(\mathbf{r}_s)$ interpolating it for the whole radial region of interest have been given in Ref. [27]. These expressions are obtained without any divergence problems in the calculations of annihilation rates over the entire range of the density parameter $\mathbf{r}_s$. $\epsilon_{\rm corr}$ is thus calculated from the ground-state expectation value of the Hamiltonian, which describes the electron gas plus the incoming positron fixed at a given distance. The analytic interpolated expressions for $\epsilon_{\rm corr}$ in the whole range of the density parameter $\mathbf{r}_s$ $[\frac{4}{3}\pi\mathbf{r}_s^3\rho(\mathbf{r})=1]$, where $\rho(\mathbf{r})$ is the undistorted electronic density of the target, are given as

$$2\epsilon_{\rm corr}(\mathbf{r}_s)=-\frac{1.56}{\sqrt{\mathbf{r}_s}}+(0.051\ln\mathbf{r}_s-0.081)\ln\mathbf{r}_s+1.14 \qquad r_s\leqslant 0.302, \quad (3)$$

$$2\epsilon_{\rm corr}(\mathbf{r}_s)=-0.923\,05-\frac{0.054\,59}{\mathbf{r}_s^2}, \quad 0.302\leqslant r_s\leqslant 0.56, \quad (4)$$

$$2\epsilon_{\rm corr}(\mathbf{r}_s)=-\frac{13.151\,11}{(\mathbf{r}_s+2.5)^2}+\frac{2.8655}{(\mathbf{r}_s+2.5)}-0.6298, \qquad 0.56\leqslant r_s\leqslant 8.0, \quad (5)$$

and, finally,

$$2\epsilon_{\rm corr}(n\mathbf{r}_s)=-179\,856.2768n^2+186.4207n-0.524, \qquad 8.0\leqslant r_s\leqslant\infty \quad (6)$$

where $n(\mathbf{r}_s)$ is the electronic density corresponding to the density parameter $\mathbf{r}_s$.

The positron correlation polarization potential (PCOP), defined as a functional derivative of the correlation energy with respect to $\rho(\mathbf{r})$, can be derived conveniently from the following equation in terms of functional derivative of the density parameter [28];

$$V_{\rm corr}(\mathbf{r})=\left(1-\frac{1}{3}\,\mathbf{r}_s\,\frac{d}{d\mathbf{r}_s}\right)\epsilon_{\rm corr}(\mathbf{r}_s). \quad (7)$$

One therefore obtains the following form of $V_{\rm corr}(\mathbf{r})$ (in atomic units) from Eqs. (2)–(7):
for $r_s\leqslant 0.302$,

$$2V_{\rm corr}(\mathbf{r})=\frac{-1.30}{\sqrt{\mathbf{r}_s}}+(0.051\ln\mathbf{r}-0.115)\ln\mathbf{r}_s+1.167; \quad (8)$$

for $0.302 \leqslant r_s \leqslant 0.56$,

$$2V_{\rm corr}(\mathbf{r}) = -0.923\,05 - \frac{0.090\,98}{\mathbf{r}_s^2}; \tag{9}$$

and, for $0.56 \leqslant r_s \leqslant 8.0$,

$$2V_{\rm corr}(\mathbf{r}) = \frac{8.7674\mathbf{r}_s}{(\mathbf{r}_s+2.5)^3} + \frac{13.151+0.9552\mathbf{r}_s}{(\mathbf{r}_s+2.5)^2} + \frac{2.8655}{(\mathbf{r}_s+2.5)} - 0.6298. \tag{10}$$

Note that for molecular systems the short-range $\epsilon_{\rm corr}(\mathbf{r}_s)$ is to be divided by a factor of $(2l+1)/\sqrt{4\pi}$ to be consistent with the single-center expansion in terms of symmetry adapted angular basis set. Here we do not worry about the $8.0 \leqslant rr_s \leqslant \infty$ region, as this range is beyond the crossing point where the polarization potential is accurately described by Eq. (1).

Thus, the PCOP potential $V_{\rm pol}^{\rm PCOP}(\mathbf{r})$ for the e^+-molecule system is given by [17]

$$V_{\rm pol}^{\rm PCOP}(\mathbf{r}) = V_{\rm corr}(\mathbf{r}), \quad r \leqslant r_c, \tag{11}$$

and by Eq. (1) for the $r \geqslant r_c$ range. Here r_c is the radius where the $V_{\rm corr}$ and $-\alpha_0/2r^4$ (or $\alpha_2/2r^4$) terms cross each other for the first time.

The new PCOP potential [Eq. (11)] has several favorable points worth mentioning here: first, it involves a true correlation of the incoming e^+ with the target electrons at short-distance encounters, and it exhibits the correct behavior in the asymptotic region; second, it is very easy to calculate and convenient to incorporate into any model potential approach; third, it is quite different from the corresponding EPP; and finally, it gives qualitatively good results on various collision observables for several atomic and molecular targets as compared with experimental data [9,10].

In our present treatment of the quantum dynamics the scattering equations are set up in the single center expansion formalism under the BF adiabatic-nuclei-rotation (ANR). We have different codes available to solve these equations for linear and nonlinear systems. In the present case of diatomic species (H_2, N_2, CO, etc.), coupled equations are solved under the integral equation method [9,10,29].

Assuming the linear molecule in its ground electronic state and with a fixed nuclear geometry, the equation of the continuum positron wave function $P(\mathbf{r}_p)$ can be written as

$$[\nabla + k^2 - 2V(\mathbf{r}_p)]P(\mathbf{r}_p) = 0, \tag{12}$$

where k^2 is the e^+ energy in Ry, and the interaction potential $V(r_p)$ includes the repulsive static and attractive polarization forces. Expanding the $V(r_p)$ in terms of Legendre projections, v_λ,

$$V(\mathbf{r}_p) = V_{\rm st}(\mathbf{r}_p) + V_{\rm pol}(\mathbf{r}_p) = \sum_{\lambda=0}^{\lambda_{\max}} [v_\lambda^{\rm ST}(\mathbf{r}_p) + v_\lambda^{\rm POL}]P_\lambda(\cos\theta), \tag{13}$$

and the continuum function $P(\mathbf{r}_p)$ for a given symmetry Λ, we obtain the following set of coupled differential equations for the fixed-nuclei (FNA) situation

$$\left[\frac{d^2}{dr^2} - \frac{l(l+1)}{r_p^2} + k^2\right] P_{ll_o}^\Lambda = \sum_{l'} V_{ll'}(r_p) P_{l'l_o}^\Lambda(r_p), \tag{14}$$

where the potential matrix $V_{ll'}$ is determined as usual. Here Λ corresponds to $\Sigma(\Lambda=0)$, $\Pi(\Lambda=1)$, $\Delta(\Lambda=2)$, $\Phi(\Lambda=3)$, etc. symmetries [30].

A polar molecule (CO) needs special attention in a BF-FNA treatment of the theory where the forward DCS's are undefined [11]. In this respect, we employ the multipole-extracted-adiabatic-nuclei (MEAN) scheme of Norcross and Padial [31], in which the DCS's for the $j \to j'$ rotational transition are given as

$$\frac{d\sigma_{(j\to j')}}{d\Omega} = \frac{d\sigma_{(j\to j')}^{\rm FBA}}{d\Omega} + \frac{kj}{4kj} \sum_{l_t} [C(jl_tj';00)]^2 \frac{1}{k^2} \times \sum_{\lambda=0}^{\lambda_{\max}} (B_{\lambda,l_t} - B_{\lambda,l_t}^{\rm FBA}) P_\lambda(\cos\theta), \tag{15}$$

where the first term is the usual closed form for the (jj') rotational excitation DCS's in the space-fixed first Born approximation (FBA), kj and kj', respectively, are the wave vectors in the initial and final channels, $C(\ )$ is a Clebsh-Gordan coefficient, l_t is the angular momentum transferred during the collision (Δj), B_{λ,l_t} are the DCS expansion coefficients, and $B_{\lambda,l_t}^{\rm FBA}$ are the corresponding quantities in the FBA evaluated in the BF frame of reference. The channel vectors are related by

$$kj'^2 - kj^2 = B[j'(j'+1) - j(j+1)], \tag{16}$$

where B is the rotational constant of the molecule in question. Finally, the expressions for the total $(\sigma_t^{jj'})$ and the momentum transfer $(\sigma_m^{jj'})$ cross sections are evaluated from Eq. (15) for any (jj') transition. Total (summed over all final rotational states j') integrated (σ_t) and momentum-transfer (σ_m) cross sections can easily be obtained from

$$\sigma_t \ \text{ or } \ \sigma_m = \sum_{j'} \sigma_t^{jj'} \ \text{ or } \ \sigma_m^{jj'}. \tag{17}$$

III. VIBRATIONAL DYNAMICS

One may relax the FNA scheme by first allowing the nuclei to move during the scattering process, thereby coupling their motion with that of the impinging positron projectile. Thus, in the BF scheme mentioned in Sec. II, one can still keep the expression over vibrational degrees of freedom such that they are dynamically linked to the positron during the scattering [32], and therefore write the total Hamiltonian as

$$\hat{H}^{\text{BF-VCC}} = \hat{H}(\mathbf{r}_p) + \hat{H}_{\rm el}(\mathbf{r}_e) + \hat{H}_{\rm vib}(\mathbf{R}) + V(\mathbf{r}_p, \mathbf{r}_e, \mathbf{R}) \tag{18}$$

where $\mathbf{r}_e$ now labels the electronic coordinates in the target, and $\mathbf{R}$ is the internuclear coordinate for the diatomic. $\hat{H}_{\rm vib}$ describes the vibrational motion in the latter system, while $\hat{H}_{\rm el}$ gives the quantum motion of its bound electrons, taken to be in their ground electronic state. The interaction potential is of the same nature as the one discussed earlier and includes now the dependence on the internuclear coordinates.

In the body-fixed-vibrational-close-coupling (BF-VCC) scheme the rotational part, $\hat{H}_{\rm rot}(\hat{\mathbf{R}})$, of the full Hamiltonian has been omitted because the employed BF frame is still rigidly fixed to the molecular target [33]. The corresponding total wave function can then be expanded in terms of vibrational states for the case of a diatomic target like CO,

$$\Psi^{\rm BF\text{-}VCC}=\chi_o(\mathbf{r}_e|R)\sum_{\nu,l}\ \phi_\nu^k(\mathbf{R})u^\Lambda_{\nu l,\nu_o l_o}(r_p)(r_p^{-1})Y_{l\Lambda}(\hat{\mathbf{r}}_p). \tag{19}$$

$\chi_o(\mathbf{r}_e|\mathbf{R})$ is the ground-state electronic wave function (parametrically dependent on $\mathbf{R}$), ϕ_ν^k is one of the vibrational wave functions of the molecule for the selected normal mode $\mathbf{k}$, and ν labels the vibrational quantum number within that manifold. $Y_{l\Lambda}(\hat{\mathbf{r}}_p)$ now denotes the angular part of the positron wave function, where l is its orbital angular momentum and Λ is the projection of l along the internuclear axis $\Lambda=\boldsymbol{l}\cdot\hat{\mathbf{R}}$. In the BF-VCC scheme for linear molecules this quantity is a good quantum number (constant of motion). The unknown function $u^\Lambda_{\nu l,\nu_o l_o}(r_p)$ is the radial part of the positron wave function, where $(\nu_o l_o)$ denotes the particular initial channel which has been selected for the vibrational and angular momenta.

One should note here that the $\chi_o(\mathbf{r_e}|\mathbf{R})$ wave function first corresponds to the undistorted electronic ground state of the target, and is thus employed to generate the exact v_λ^{st} coefficients of Eq. (13). However, it is then distorted by the phenomenological correlation potential discussed before in order to provide the $v_\lambda^{\rm POL}$ coefficients of Eq. (13). Thus, one should, more correctly, consider expansion (19) as being given over some ''effective'' target electronic wave function which is initially built via the asymptotic target electronic wave function and then modified to yield the final interaction. Were we to use a conventional configuration-interaction expansion to obtain correlation-polarization effects, then Eq. (19) will include a further sum over several eigenfunctions of $\hat{H}_{\rm el}(\mathbf{r}_e)$.

Now using Eqs. (18) and (19) in the Schrödinger equation (14), one obtains the corresponding BF-VCC coupled differential equations

$$\left\{\frac{d^2}{dr_p^2}-\frac{l(l+1)}{r_p^2}+k_\nu^2\right\}u^\Lambda_{\nu l,\nu_o l_o}(r_p)$$

$$=2\sum_{\nu' l'}\ V^{\Lambda,k}_{\nu l,\nu' l'}(r_p)u^\Lambda_{\nu' l',\nu_o l_o}(r_p), \tag{20}$$

with

$$V^{\Lambda,k}_{\nu l,\nu' l'}(r_p)=\sum_\lambda\ \langle\phi_\nu^k(R)|V_\lambda(r_p|R)|\phi_{\nu'}^k(R)\rangle g_\lambda^\Lambda(ll') \tag{21}$$

and

$$g_\lambda^\Lambda(ll')=\left\{\frac{2l'+1}{2l+1}\right\}^{1/2}C\begin{pmatrix}\lambda & l' & l\\ o & \Lambda & \Lambda\end{pmatrix}\begin{pmatrix}\lambda & l' & l\\ o & o & o\end{pmatrix} \tag{22}$$

and

$$k_\nu^2=2(E-\boldsymbol{\epsilon}_\nu^k), \tag{23}$$

$\boldsymbol{\epsilon}_\nu^k$ being the energy of the νth vibrational state within the kth mode. V_λ is obtained in turn from the following expression:

$$\langle\chi_o(\mathbf{r}_e|\mathbf{R})|V_{p\text{-mol}}(\mathbf{r}_p,\mathbf{r}_e,\mathbf{R})|\chi_o(\mathbf{r}_e|\mathbf{R})\rangle$$

$$=\sum_\lambda\ V_\lambda(r_p|R)P_\lambda(\hat{\mathbf{r}}_p\cdot\hat{\mathbf{R}}). \tag{24}$$

The C's of Eq. (22) are the usual Clebsh-Gordan coefficients. The vibrational wave functions of the molecule can be obtained first by solving the following differential equation for each of the normal coordinates R_k;

$$\left\{\frac{d^2}{dR_k^2}+2\mu[\boldsymbol{\epsilon}_\nu^k-U_k^o(R_k)]\right\}\phi_\nu^k(R_k)=0, \tag{25}$$

where μ is the reduced mass of the molecule, and $U_k^o(R_k)$ comes from the ground electronic state Ψ_o of the target which provides the potential supporting, for each kth normal mode, the corresponding vibrational bound states.

The solution of the coupled equations (20), subject to the usual asymptotic boundary conditions, finally yield the T matrix $T^\Lambda_{\nu l,\nu_o l_o}$, and from this we can obtain the partial integral vibrational excitation cross section using the expression [34]

$$\sigma_k(\nu_o\rightarrow\nu)=\frac{\pi}{k_\nu^2}\sum_\Lambda\ \sum_{ll_o}\ |T^\Lambda_{\nu l,\nu_o l_o}|^2 \tag{26}$$

for each of the kth normal modes of interest. Only one is obviously present for CO.

When the energy of the incoming positron is such that the energy spacing between rotational levels is only a small fraction of the total energy, then the molecule is considered to be nonrotating, and the BF-VCC method states that the vibrational motion of the molecule and the angular momentum of the positron are coupled via the $V^{\Lambda,k}_{\nu l,\nu' l'}$ potential only. The scattering process, therefore, treats the actual dynamical coupling between the vibrational modes of the molecule and the ''local'' kinetic energy of the impinging positron as acting during the evolution of the scattering state in Eq. (20) for each of the molecular normal modes. This is therefore a better approximation than the simpler vibrational adiabatic approach [35], whereby the convolution over vibrational levels, initial and final, is carried out only after the fixed nuclei rotation problem has been solved for each value of $R_{\mathbf{k}}$ (see also Elza *et al.* [22]). We shall further see below that this more correct dynamical coupling is an essential ingredient for the evaluation of possible threshold peaks in the vibrationally inelastic channels.

We have also recently examined [9] an approximate formulation for Eq. (22) which can be obtained by further considering each value of the positron angular momentum $\hat{l}$ as being conserved during the collision. If one further combines this simplification of the helicity decoupling [36] within the scattering process with the assumption that the rotational energy losses occurring during collision could be considered small when compared with the magnitude of the initial wave-

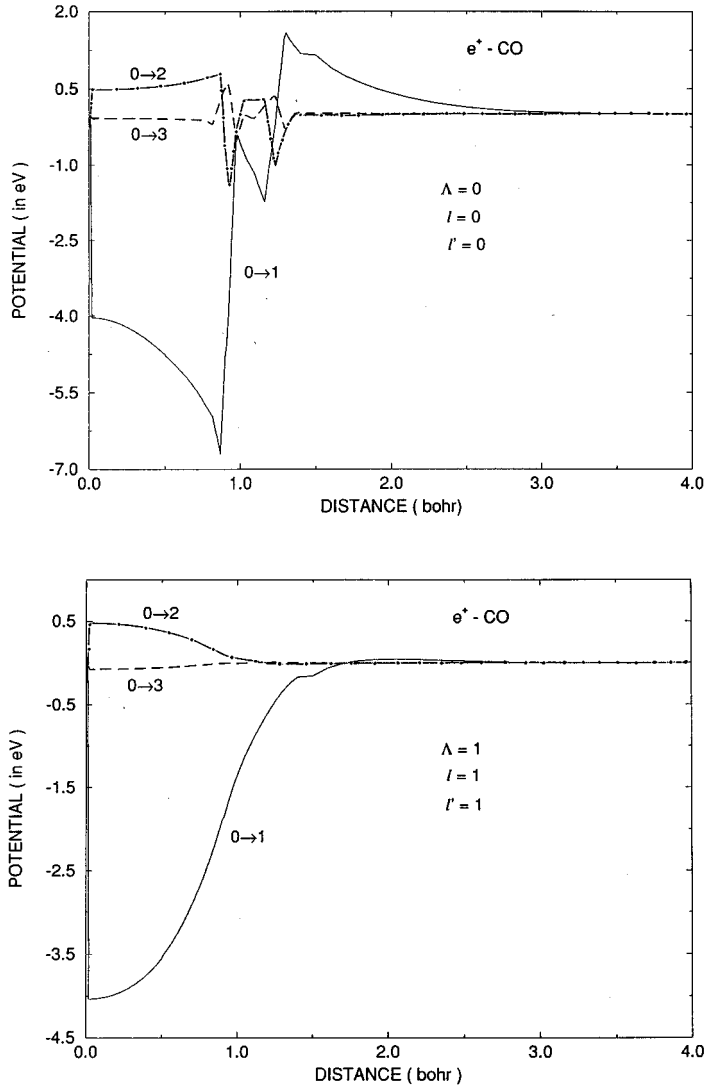

FIG. 1. Computed coupling potential terms between vibrational levels of the CO target and as a function of the relative distance of the positron. Top: Σ-scattering; bottom: Π-state scattering.

vector values, then one finds that the previous BF-VCC coupling scheme is reduced to a simpler version in which the coupling originating from the positron angular momentum is treated adiabatically. We call this simpler version the adiabatic angular momentum coupling (AAMC) scheme, and have discussed its derivation in detail earlier [9]; therefore we will not be repeating it here.

The BF-VCC coupled equation (20) and the coupling potential of Eq. (21) show that the orbital angular momenta of the positron motion are coupled through the angular part of the effective potential $g_\lambda(ll')$. Thus, in the BF-VCC equations this geometric factor acts dynamically during the scattering processes. On the other hand, the BF-VCC–AAMC coupled differential equations [9] show that the angular momentum of the positron is no longer coupled via the full effective potential of Eq. (22), and therefore the scattering solutions are uncoupled with respect to their angular momentum, which is in turn treated as a separate constant of motion, while one still has vibrationally coupled equations as in the BF-VCC treatment. The effect of the geometric factor $g_L(ll_o)$ on the scattering cross section now appears to be modified in the BF-VCC–AAMC scheme, and does not act dynamically during the actual collision process but only in an adiabatic way by remaining fixed during each trajectory. In sum, we could say that in the BF-VCC scheme the vibrational motion of the nuclei, via the electronic charge distribution of the molecule, is dynamically coupled to the motion of the positron, while in the BF-VCC–AAMC approximation the vibrational motion remains only adiabatically coupled to the motion of the positron. The complex recoupling of both partners' angular momenta during the dynamics is thus simplified by an adiabatic treatment for each value of $\hat{l}$ [9,10]. However, in previous work we have already shown that such a simplification, although found to be useful and fairly realistic for neutral systems interacting via van der Waals forces [37], turns out to be too weak for describing the dynamical coupling of a charged quantum probe like the positron projectile at low scattering energies [9,10].

A. Coupling potentials

In order to give a more precise feeling of the behavior of the coupling forces during the scattering process, in Figs. 1 and 2 we show the radial parts of the potentials given by Eq. (21). The employed target wave functions at the various R values are those given long ago by McLean and Yoshimine [38], and with those values one is able to span the first five vibrational levels of the CO target by numerically generating

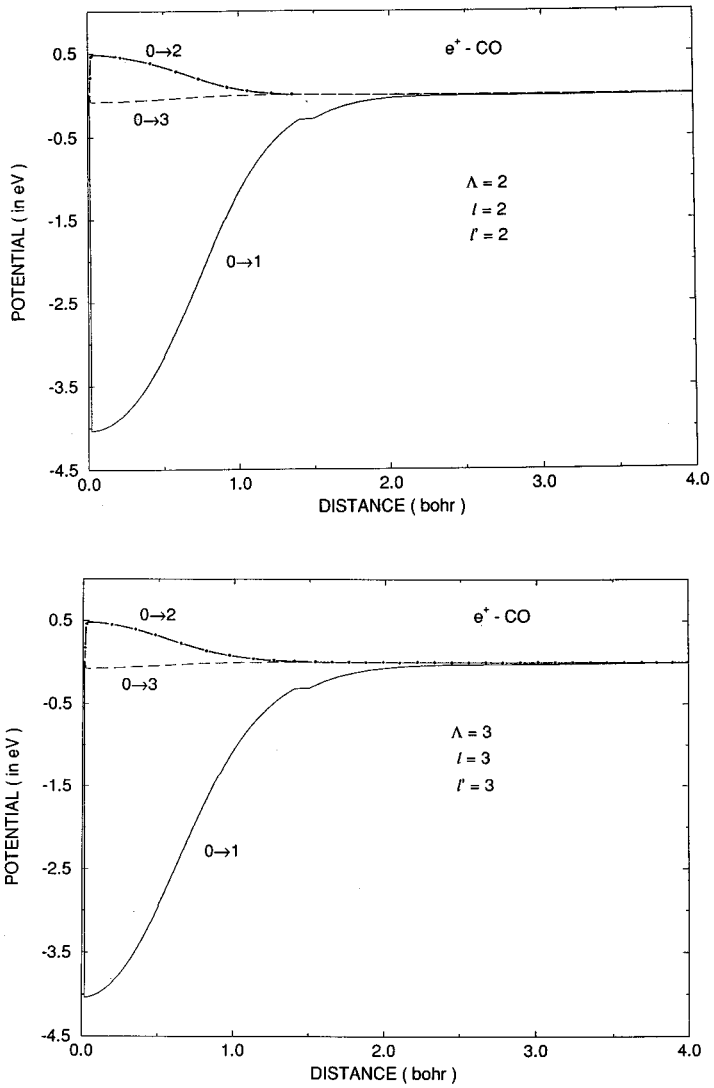

FIG. 2. Same as in Fig. 1 but for Δ scattering (top) and Φ scattering (bottom). The various vibrational transitions are shown next to each curve.

the bound-state wave functions. The values of Λ which were generated for the scattering states went up to $\Lambda=13$, keeping both odd and even values. The maximum value of the partial wave in Eq. (21) was $l_{\max}=20$, and the multipolar potential of Eq. (13) was expanded up to $\lambda=16$. The radial integration over τ_p, because of the dipole interaction present in this system, was extended up to $r_p=230$ bohr. The corresponding vibrational energy spacings found here were (in eV) $\Delta\epsilon_{01}=0.266$, $\Delta\epsilon_{02}=0.528$, $\Delta\epsilon_{03}=0.787$, and $\Delta\epsilon_{04}=1.043$.

Figure 1 shows two of the scattering states, $\Lambda=0$ and 1, for which the coupling potentials were computed: the top part of the figure corresponds to Σ-state scattering, while the lower part refers to Π-state scattering. The different vibrational levels, being coupled by the potentials, are indicated for each curve; the (l,l') indices further refer to the partial waves of the scattering equations which are directly coupled by the potential terms. It is interesting to note that the $\Delta\nu=1$ terms, from the ground vibrational level $\nu=0$, are by far the strongest coupling terms, and extend over the larger range of radial distances: multiple, direct excitations of vibrational levels by positron scattering are clearly less favored by the coupling potentials.

In Fig. 2 the coupling results are shown for Δ and Φ scattering states and for the same range of excitation processes; the (l,l') terms are always those associated with the lowest allowed values for that specific scattering state. One clearly sees once more that $\Delta\nu=1$ coupling terms are by far the strongest, and that they extend over the largest range of radial values in comparison with $\Delta\nu\geqslant 1$ couplings. Furthermore, the coupling is essentially located at very short distances from the c.o.m. of the target molecule, and dies out very rapidly as the positron moves outside the molecular charge distributions. That the inelastic vibrational coupling is here found to be fairly short ranged in nature and dominated by $\Delta\nu=1$ transitions will be seen to have marked effects on the features of the computed inelastic vibrational cross sections.

B. Inelastic cross sections

The behavior of the partial integral cross sections of Eq. (26) is shown, in fact, by the calculations reported in Fig. 3 over the range of collision energies below the formation of Ps states. The largest cross section is given by the $\sigma(0\rightarrow 1)$ excitation process, which is still, however, rather small compared with the electron-CO results at the same energies [39]. The following comments can be easily made.

(i) The multiple excitation processes ($\Delta\nu=2$, 3, and 4) show cross sections which are markedly smaller than those

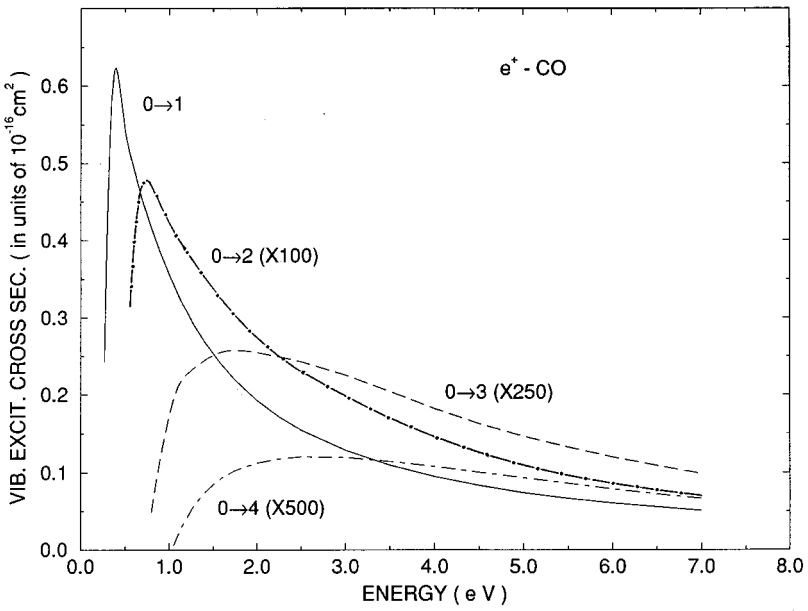

FIG. 3. Computed partial integral vibrationally inelastic cross sections for different excitation processes, as a function of collision energy. The factors indicated for some of the processes show their enlargements in order to be in the same scale as the $(0\rightarrow 1)$ process.

from the single-jump excitation collision: the reduction in size is of two orders of magnitude for $\Delta\nu=2$, and increases to more than three orders of magnitude at the threshold opening for the $\Delta\nu=4$ process. This feature indicates that, although the interaction between the low-energy positron and the molecular charge distribution is not weak, and usually is seen to induce sizable deformations of the total electron density, it appears to be less able to alter the electron density in the inner region involved in the chemical bond formation as the impinging probe mainly samples the outer region of the molecular formation target at the low collision energy considered here.

(ii) The $(0\rightarrow 1)$ excitation cross section here, on the other hand, is remarkably larger than that shown by nonpolar targets like H_2, N_2 [9], and CO_2 [10]. At the collision energy just above the opening of the $\nu=1$ threshold (0.266 eV), in fact, the corresponding inelastic cross section is two orders of magnitude larger than in the case of the excitation process for the symmetric stretching made in the CO_2 target [10]. Thus one can see fairly clearly that the dipole interaction (and its dependence on the molecular vibration) provides a strong, long-range contribution which affects the vibrational excitation process, in spite of its dominant short-range features, when the collision occurs in the neighborhood of the threshold energy.

(iii) The presence of the marked peak at the threshold is also in keeping with what has been suggested in collisions of electrons with polar molecules and in the excitations of their vibrational modes at very low energies [40–43], where it was surmised that the Born point-dipole approximation could be responsible for the rapid onset of the cross section and for its rapid falloff with increasing energy. We see that the present treatment of the coupled dynamics for positron scattering strongly suggests that a similar process should occur for the threshold collisions of such projectiles with polar molecules, in spite of the weaker coupling that positrons ex-

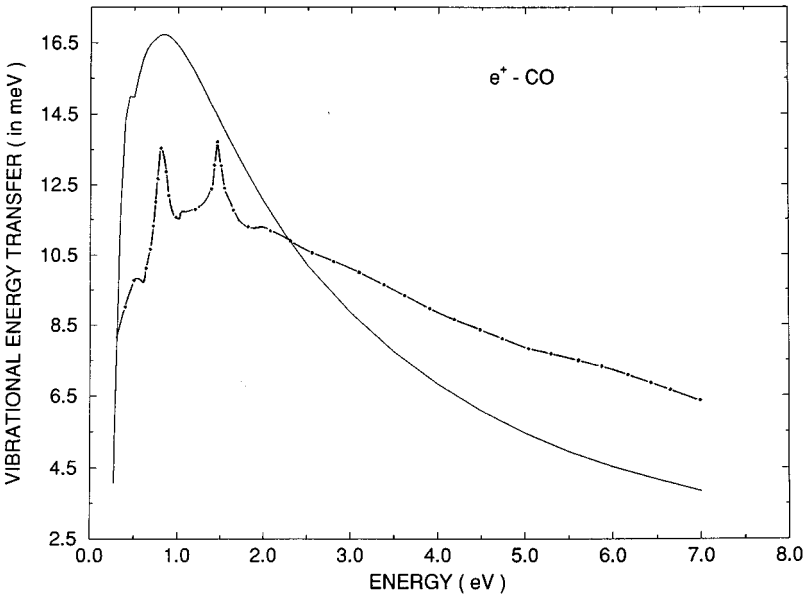

FIG. 4. Computed vibrational energy-transfer values as a function of collision energy. The solid line shows the BF-VCC results discussed in the main text, while the dash-dotted line shows the simpler BF-VCC-AAM coupling calculations, also discussed in the main text.

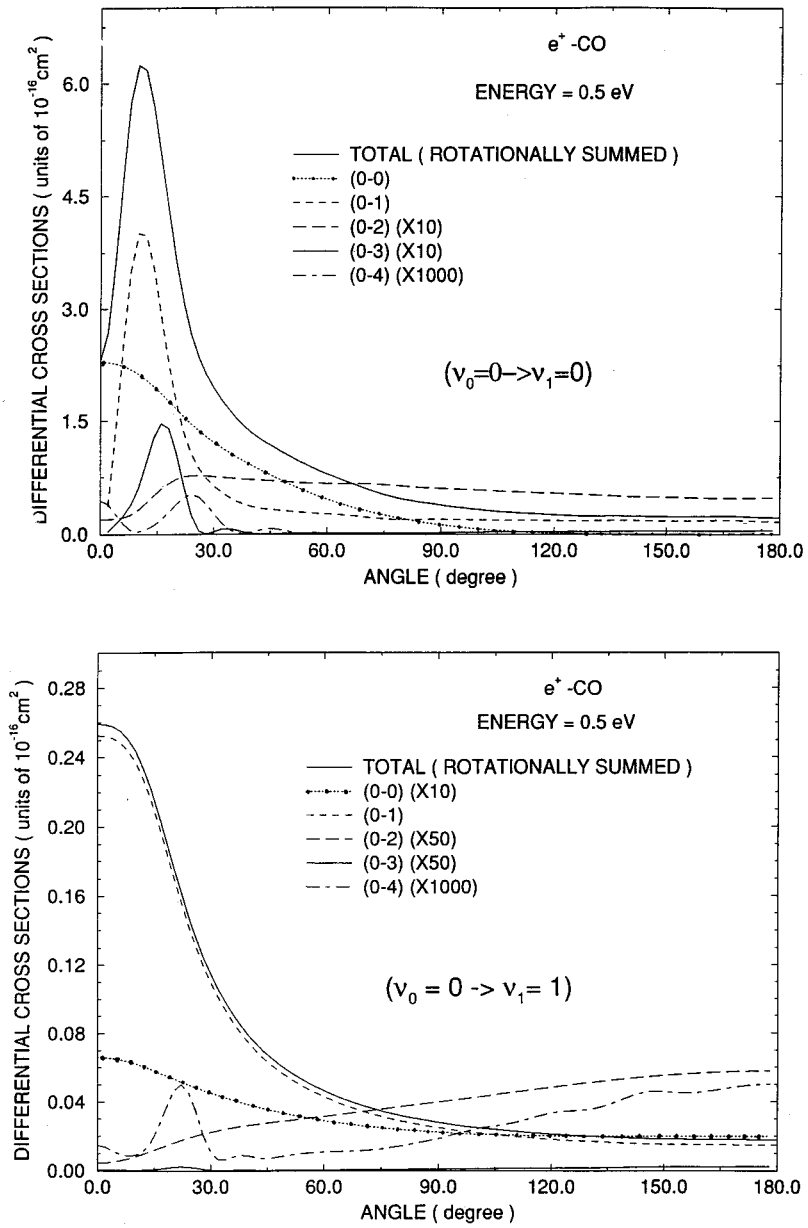

FIG. 5. Differential cross sections at 0.5 eV of collision energy. Top: state-to-state rotationally inelastic DCS's within the vibrationally elastic process. Bottom: same as the top, but for the vibrationally inelastic process.

hibit, with respect to electrons, in their interactions with molecular vibrational modes.

Another useful indicator of the relative efficiency of rotationally and vibrationally inelastic collisions is given by the evaluation, out of a selected rotational-vibrational level of the target molecule, of the average energy transfer index defined as

$$\langle \Delta E \rangle = \sum_{i=o}^{\infty} \sigma_{o\to j} \Delta \epsilon_{oj} \Big/ \sum_{i=o}^{\infty} \sigma_{o\to j}, \tag{27}$$

where $|j\rangle$ is the index of each final rotational or vibrational level which is being considered, and $\Delta \epsilon_{oj}$ the corresponding energy spacing (in meV). The indicator can be directly evaluated for the vibrational energy by considering, at each given energy, that the rotationally summed cross sections are decoupled from vibrationally inelastic collisions, since they occur on a much slower time scale than the latter excitations. The results for such a quantity from the molecular initial vibrational level $\nu=0$ are shown in Fig. 4. The solid line shows the calculations carried out using the BF-VCC equation (21), while the dash-dotted line refers to the results obtained by using the more approximate coupling, the BF-VCC–AAMC equation mentioned before [9].

We see that both calculations exhibit a strong maximum region at low energies, although the more approximate coupling causes the cross section to present strong additional peaks at the opening of the second threshold which are also given, but much smaller in size, by the correct coupling dynamics of Eq. (21). In other words, the full angular momentum recoupling of Eq. (21) indicates that the dipole-supported excitation processes are the dominant ones for this polar target, and therefore they also dominate the energy-transfer efficiency in the low-energy region. The other interesting feature of the vibrational energy-transfer values reported in Fig. 4 is that the size of such average energy-transfer processes is remarkably larger than that from other, nonpolar targets: the value at the peak is more than two

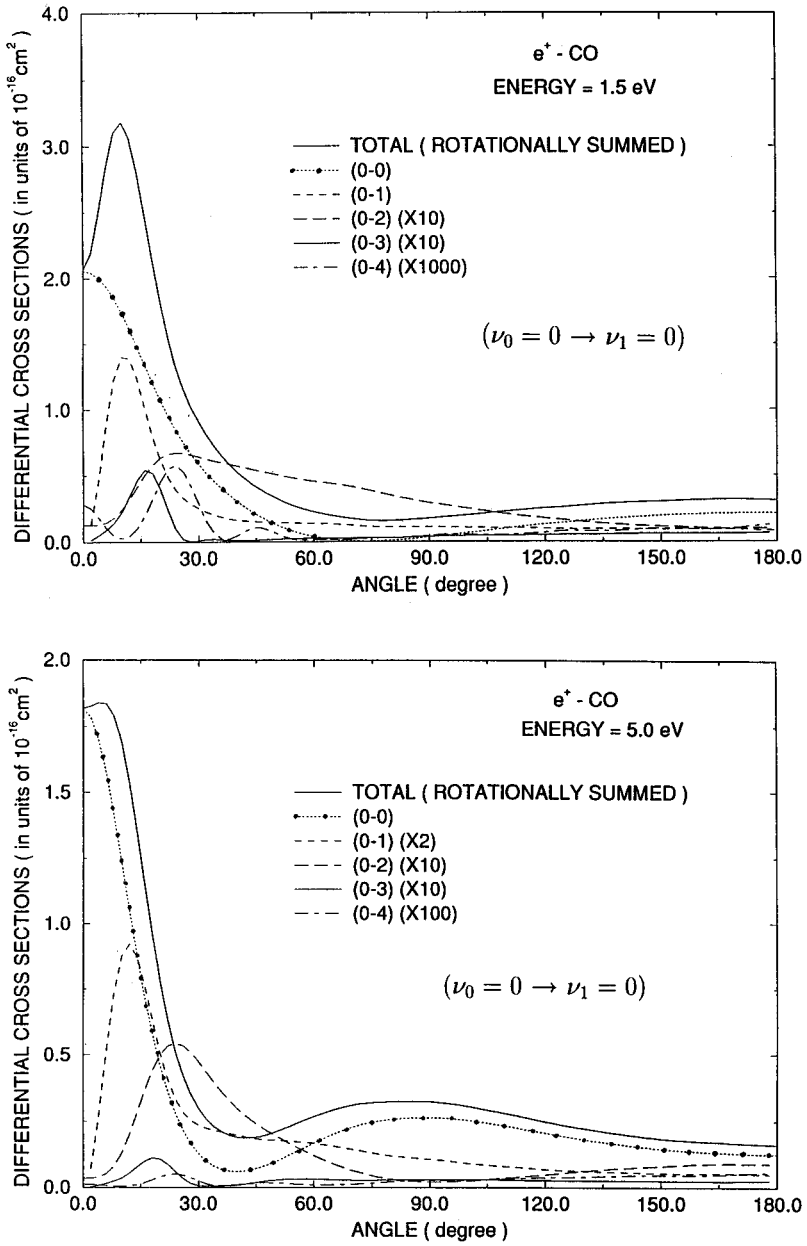

FIG. 6. Computed state-to-state DCS's, as in the top diagrams of Fig. 5, but for two different energies 1.5 (top) and 5.0 eV (bottom).

orders of magnitude larger than in CO_2 [10], and similar to the values from electron-scattering processes [39].

IV. COMPUTED ANGULAR DISTRIBUTIONS

As discussed in the previous sections, the BF calculations of the elastic (rotationally summed) differential cross sections diverge logarithmically in the forward direction [44], and require correction from the Born approximation as given by Eq. (15). Furthermore, the evaluation of rotationally inelastic cross sections has been shown to eliminate the divergence in the BF frame [32], where vibrationally inelastic processes are obtained from close-coupled (CC) equations as discussed in Sec. III. It is therefore of some interest to actually verify through accurate computations how such angular distributions for inelastic transitions behave at various collision energies.

As an example, for the low-energy regimes, not far above the opening of the $\nu=1$ vibrational threshold, in Fig. 5 we show calculations at a collision energy of 0.5 eV. The upper part of the figure presents results for rotationally inelastic processes within the vibrationally *elastic* channel, while the lower part of the same figure shows the partial differential cross sections for rotovibrationally inelastic excitations. All results have been corrected by using the Born correction as in the MEAN approximation [31] given by Eq. (15). One can make the following direct comments.

(i) The vibrationally elastic partial cross section are, as expected, larger than the rotovibrationally inelastic angular distributions. Within each manifold we also see that the $(0\rightarrow1)$ rotational excitation process, the one dominated by charge-dipole interaction, provides the largest rotationally inelastic cross section.

(ii) In the small-angle scattering region the $(0\rightarrow1)$ rotational excitation is also larger than the elastic process in both sets of cross sections, where such an effect is much more marked in the case of rotovibrational inelastic collisions (lower part of the figure);

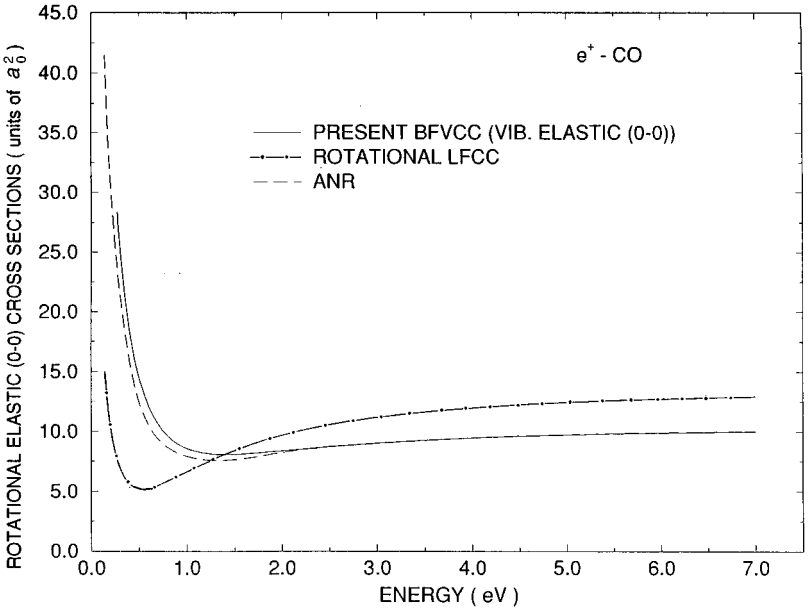

FIG. 7. Rotationally elastic integral cross sections as a function of collision energy. Solid line: BF-VCC calculations for the vibrationally elastic process. Dashed line: rigid-rotor BF calculations used within the ANR scheme. Dot-dashed line: space fixed, rigid rotor calculations (LFCC) from Ref. [46]. All values in a_0^2 units.

(iii) The ANR approximation, employed here to obtain rotationally inelastic cross sections from the BF-VCC K-matrix elements, also indicates that multiple rotational transitions have a much smaller probability than the $(0\rightarrow 1)$ excitation, which is dipole dominated. One therefore explicitly sees evidence of the different behavior of positrons as molecular probes: their repulsive interaction with the target causes the excitation to be dominated, at the energies considered, by long-range forces, and therefore the weaker, higher multipoles yield smaller excitation cross sections.

The above features of the rotationally inelastic processes obtained within the elastic channel of the BF-VCC calculations are further shown by the results reported in Fig. 6: the rotationally inelastic differential cross sections (DC are shown there for two different collision energies) at 1.5 (top) and 5.0 eV (bottom).

As the positron penetrates more deeply into the molecular charge distribution we see that the dominance of the $(0\rightarrow 1)$ rotationally inelastic DCS's is markedly reduced. The elastic process becomes strongest in the forward-scattering region, and dominates the rotationally summed angular distributions.

As mentioned in the previous sections, the MEAN approximation, i.e., the Born-corrected form of the partial DCS's [19,31] for the state-to-state inelastic cross sections, can be applied either to the FNA calculations via the ANR adiabatic scheme [35], or to the BF-VCC calculations. It therefore becomes of interest to carry out numerical tests of the different behaviors of the inelastic cross sections produced by the use of the different coupling schemes.

V. ROTATIONALLY INELASTIC PROCESSES

Because of the local nature of the PCOP interaction discussed above, one can also compute the rotationally inelastic cross sections by using a laboratory-fixed (LF) frame of reference, and then treat the scattering problem within the familiar CC expansion over rotational states of the target [45]. Recent calculations which followed the above scheme (LFCC) have been carried out for positron-CO rotationally inelastic collisions [46], and employed the same target wave function and positron-molecule interaction described in the present work: it therefore becomes of interest to compare the various results from the different coupling directly, in order to better assess the relative reliability of the various schemes. The behavior of the rotationally and vibrationally elastic $(00\rightarrow 00)$ cross section, for example, is shown in Fig. 7, and it is compared with earlier calculations that did not employ the BF-VCC scheme of the present work.

The solid line reports the present calculations which were obtained by applying the ANR approximation to the vibrationally elastic channel K-matrix elements of the BF-VCC results. The dashed line, on the other hand, shows the rigid-rotor calculations which directly used the ANR approximation with the FNA K-matrix elements [17]. One sees that both procedures produce essentially the same results over the whole range of energies, with small differences at the opening of the vibrational threshold. Considering that the two sets of results were obtained with different codes, although using the same target wave function and the same PCOP potential, the agreement found here is a confirmation of the reliability of the ANR computations even when vibrationally coupled equations are solved for the scattering of positrons. Hence, these results give us a further indication of the fairly weak coupling between positron projectiles, below Ps formation, and molecular vibrational motion.

The space-fixed (SF) calculations which solved the rigid-rotor coupled equations (LFCC) are also reported in the figure, and result from Ref. [46]. In those computations the same target wave function and the same PCOP interaction were also employed. The general shape of the cross-section dependence on collision energy is rather similar to our present results, while differences in the value appear in the low-energy region below about 1.0 eV. The LFCC calculations included ten rotational states in the scattering wave-function expansion, and up to $J_{\mathrm{tot}}=11$ in the angular momentum expansion. Although their convergence tests were rather limited, it is reasonable to assume that their final cross sections were within less than 5% from the converged results

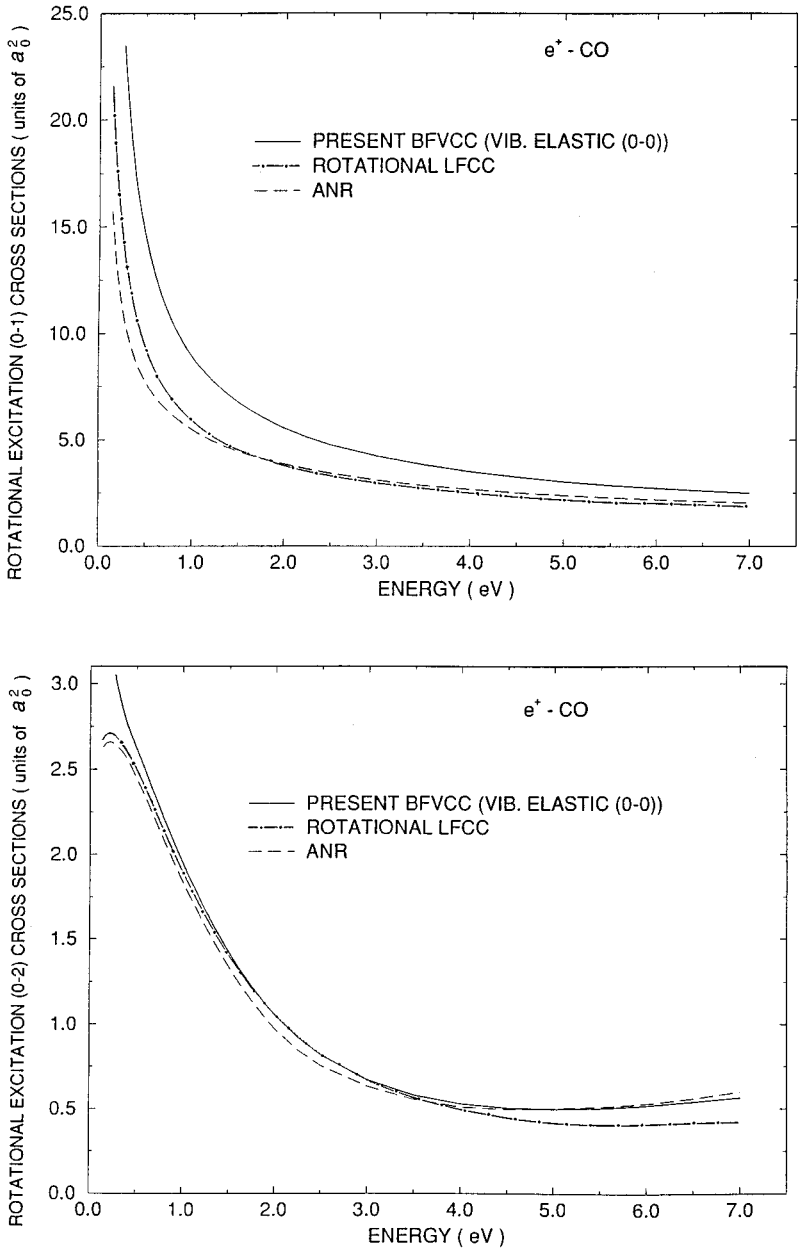

FIG. 8. Rotationally inelastic, partial integral cross sections within the vibrationally elastic channel. The meaning of symbols is the same in Fig. 7. Top: $(0\rightarrow1)$ excitation. Bottom: $(0\rightarrow2)$ excitation. All values in a_0^2 units.

[46]. The analysis of the other LFCC partial cross sections show that below 1.0 eV the rotationally inelastic processes are the main contributors to the total cross sections, since the existence of the rotating dipole moment produces the largest dynamical effects as the energy becomes smaller. Hence one can say that the ANR results are not treating the dynamics in that range of collision energy realistically.

The interplay between rotational dynamical coupling and the relative strength of the various multipolar coefficients of the interaction potential can be seen more clearly from a comparison between partial, rotationally inelastic cross sections within the vibrationally elastic channel which we have displayed in Figs. 8 and 9. The upper part of Fig. 8 shows, in fact, the $(0\rightarrow1)$ rotational transition computed, using Born-corrected results, from both the BF-VCC equations and the ANR transformation from the FNA equations. The results from the SF dynamics of the rigid-rotor excitation (LFCC) are also shown by the dot-dashed line.

It is interesting to see there that the rotationally inelastic process most directly given by dipole coupling is obtained rather reliably from Born-corrected ANR results down to low collision energies below 1.0 eV. As expected, the two sets of rigid-rotor calculations (ANR and LFCC) are essentially identical, as also suggested by previous tests on H_2 [47], as the collision energy increases and as the dynamical simplifications implied by the ANR scheme become more acceptable. On the other hand, the inclusion of the vibrational coupling and of the dependence of the dipole moment on the internuclear distance plays a rather important role here, as opposed to the rotationally elastic case discussed in Fig. 7, and therefore the size of the inelastic cross sections is modified rather markedly at all energies.

As one moves to the weaker quadrupole moment coupling for the $(0\rightarrow2)$ direct excitation process, the results of the comparison change as shown in the lower part of Fig. 8. The inclusion of vibrational coupling is now less important in the long-range region, and therefore the BF-VCC and ANR results nearly coincide at all energies. They are also very close

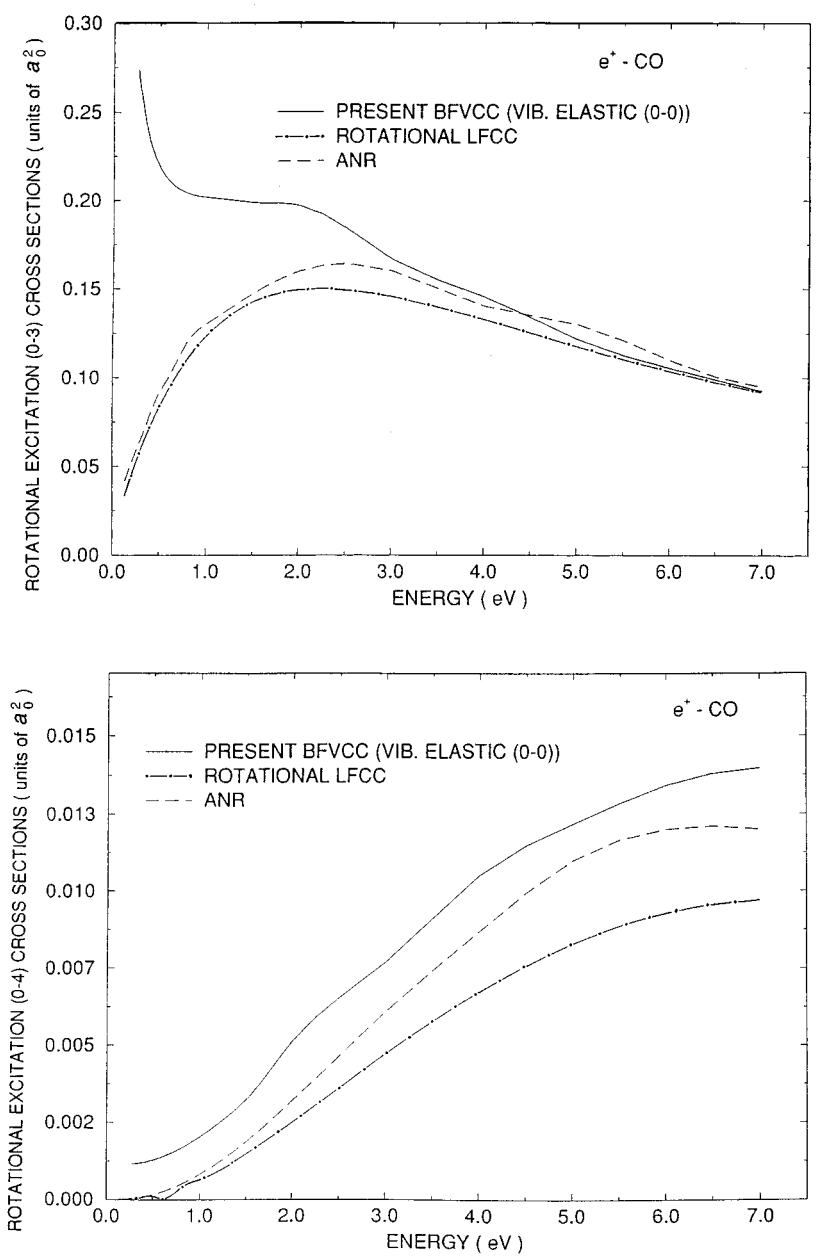

FIG. 9. Same as in Fig. 8 and with the same meaning of the symbols. Top: $(0\rightarrow3)$ excitation. Bottom: $(0\rightarrow4)$ excitation. All quantities in a_0^2 units.

to the LFCC calculations where only very-low collision energies ($\leqslant 0.1$ eV) appear to affect the validity of the ANR scheme, and to indicate differences due to the vibrational coupling. The discrepancies of high collision energies from the LFCC results could be due to their lack of convergence as more rotational channels become open.

The results relative to $(0\rightarrow3)$ and $(0\rightarrow4)$ rotationally inelastic partial cross sections are further reported in the upper and lower parts of Fig. 9, respectively. The ANR and LFCC results for the rigid-rotor calculations are again fairly similar in their energy dependence, but show some discrepancies in terms of their relative size. The ANR results are invariably larger than the close-coupled calculations, possibly suggesting that the latter are still not converged for these excitation processes with $\Delta j \geqslant 1$.

Furthermore, the same inelastic cross sections, extracted via the ANR scheme from the BF-VCC elastic K matrix, are reported by the solid lines, and behave differently from the previous results. Such differences appear to suggest that vibrational coupling plays an increasingly important role as higher excited rotational states are reached by collision, and therefore one should take the simpler ANR results as only qualitative findings for such processes. Obviously, rotovibrational coupling is bound to increase for a faster rotating target, and we should expect that the vibrational motion is dynamically more coupled to the impinging positron's motion when the target is also rotationally excited.

A more general comparison between experiments and theoretical results is finally shown in Fig. 10. In the main figure we report the results of the rotationally and vibrationally summed total integral cross sections obtained from the BF-VCC calculations described in this work (solid line). We also report the rigid-rotor, ANR calculations of Ref. [17] (dashed line) and the rigid-rotor, close-coupled calculations in the space-fixed LFCC results from Ref. [46] (dot-dashed lines). The corresponding experimental results are given by the

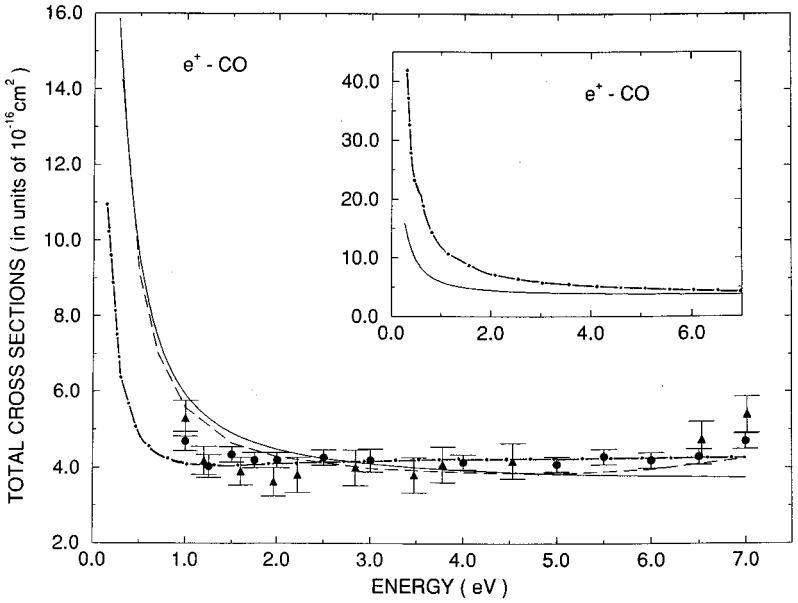

FIG. 10. Total integral cross sections below the Ps formation threshold. Main figure: solid line, present BF-VCC calculations; dashed line, BF rigid-rotor ANR calculations [17]; dot-dashed line, space-fixed rigid-rotor close-coupled (LFCC) calculations from Ref. [46]. Inset: present BF-VCC, solid line; BF-VCC-AAM, dot-dashed line. The experiments are as follows: filled circles from Ref. [13]; filled triangles from Ref. [14].

filled circles [13] and by the filled triangles from Ref. [14]. Whenever possible, the corresponding error bars are also reported. In the inset we show the effect of simplifying the vibrational coupling by resorting to the CS approximation as discussed by us in Ref. [9]. The BF-VCC results are given by the solid line again, while the BF-VCC–AAMC calculations are given by the dot-dashed line.

As expected, the inclusion of vibrationally inelastic processes has a rather small effect on the integral total cross sections because of the smallness of the excitation probabilities shown in the previous analysis. Thus the computations given by the BF-VCC approach and those produced by the rigid-rotor ANR scheme come very close to each other at low collision energy: they begin to differ as the collision energy increases, and therefore as the vibrationally inelastic process becomes more important and subtracts flux to purely rotationally inelastic excitations. The space-fixed calculations, on the other hand, are very different at very low energies, and indicate clearly the dynamical effects arising from correctly coupling the positron motion with the long-range forces of the polar target. Such effects are reduced as the collision energy increases, and therefore the dash-dotted curve follows more closely the BF results given by the other two calculations. On the whole, however, we see that the present calculations agree well with the available experiments, and describe the full rotovibrational dynamics markedly better than the earlier R-matrix calculations [16], where correlation forces produced by a more conventional configuration-interaction expansion were still not yet well described in the intermediate range of interaction.

VI. SUMMARY AND CONCLUSIONS

In the present study, we have analyzed the relative importance of various low-energy excitation processes which can occur in collisions of positrons (below the threshold of Ps formation) with polar molecules, and have focused on e^+-CO collisions up to about 7 eV of collision energy.

In particular, we have explicitly included the dynamical coupling between the motion of the projectile and the vibrational coordinate and evaluated the size of the vibrationally inelastic processes in such collisional events. Furthermore, we have included the Born correction for the well-known pathological behaviour of the dipole interaction in a BF-FN frame of reference, and extracted both elastic and inelastic angular distributions, providing rotationally inelastic transitions within a vibrational manifold.

The efficiency of the vibrational energy-transfer process turns out to be rather low for positron scattering, as expected from the physics of the interaction, but still shows a marked increase at the opening of the vibrational channel and up to about 1 eV of collision energy. This effect could be attributed to the possible presence of a long-range trapping of the positron at the threshold opening, as seen in vibrationally inelastic processes from electron scattering off polar targets [40,41,42], and as also expected to occur for positron scattering [6].

In the calculations, the theoretical values of the multipole terms were employed to generate the cross sections, as opposed to using the experimental values of the dipole and quadrupole terms. Such differences are really rather unimportant for the whole picture of the processes at hand, and one can easily check this point by comparing both sets of results, as given in Fig. 11.

In this figure we report the partial, state-to-state rotationally inelastic cross sections (top) and the corresponding momentum-transfer cross sections (bottom) as a function of the transferred rotational angular momentum Δj. The energy being considered is 1.5 eV. We see three different types of computations: the BF-VCC results with the theoretical multipoles (solid line), the rigid rotor results within the ANR approximation using the theoretical values for the multipoles (dashed lines), and the same ANR results using the experimental multipoles (dotted lines). In the last two calculations

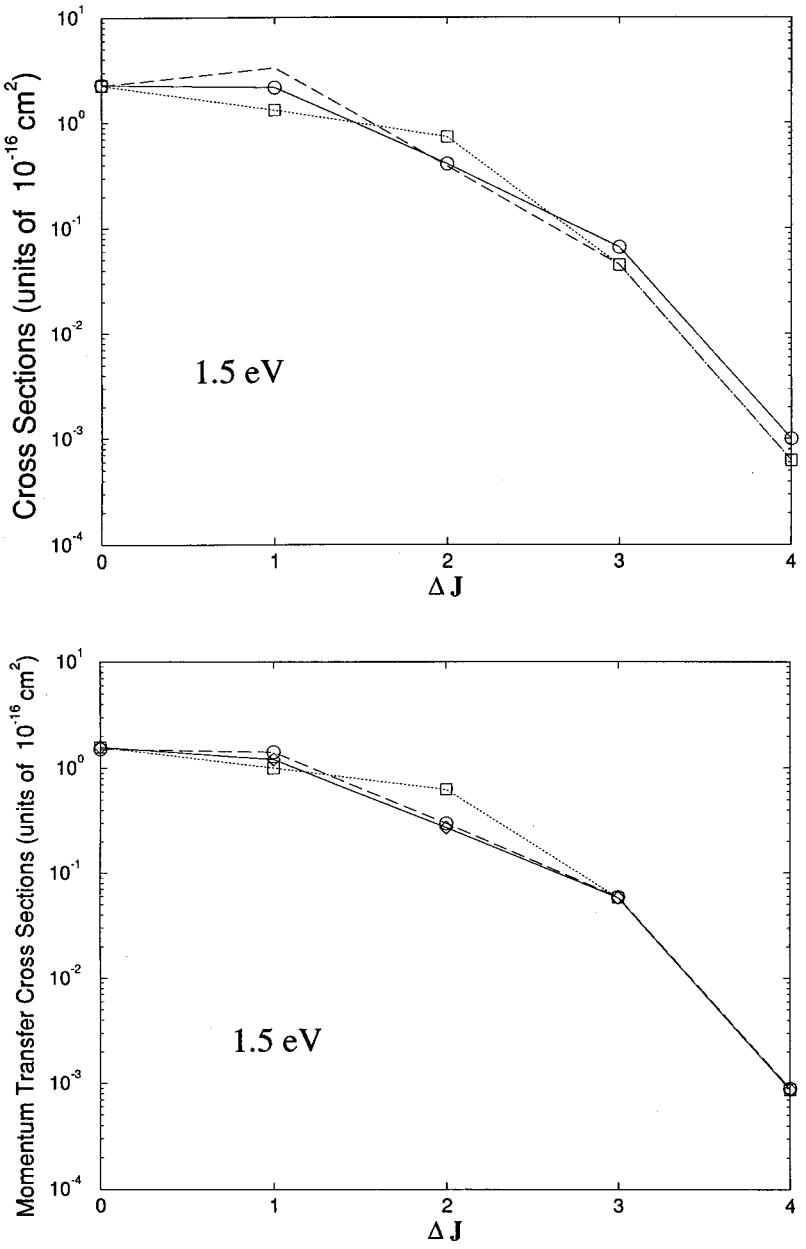

FIG. 11. Computed rotationally inelastic partial cross sections as a function of the transferred rotational angular momentum Δ_j. Solid line, BF-VCC with theoretical multipoles; dashed line, BF-ANR results with theoretical multipoles; dotted line, BF-ANR results with experimental multipoles. Top: integral cross sections. Bottom: momentum-transfer cross sections.

the Born (MEAN) correction was applied, while the BF-VCC results do not need such a correction [32].

We clearly see in both sets of calculations shown in Fig. 11 that the use of the correct dipole makes a small difference in the cross sections with $\Delta j = 1$, as expected, but has no effect on the momentum-transfer cross sections (σ_m). Furthermore, we see there that the quadrupole term changes are enhanced by the σ_m weighting of the larger angles, but again make little difference in the cross sections.

In conclusion, a comparison of the present computed integral cross sections with the available experiments shows that our treatment of the dynamics in the Born-corrected BF approach, and our modeling of correlation forces, provide, for the CO target, one of the best available accords with the measured data down to very low collision energies. It also gives us a more quantitative feeling of the relative importance of rotational and vibrational energy-transfer processes in positron scattering from molecular targets. Last, but not least, the VCC treatment clearly shows the presence of marked threshold effects and of possible positron trapping by the molecule during the inelastic dynamics.

ACKNOWLEDGMENTS

The financial support of the Italian National Research Council (CNR) and of the Italian Ministry for Universities and Research (MURST) is gratefully acknowledged. One of us (T.M.) also thanks the CNR for financial support. Finally, F.A.G. wishes to thank the kind hospitality of the Max-Planck Society in Göttingen, where this work was completed.

[1] *Atomic Physics with Positrons*, edited by J. W. Humbertson and E. A. G. Armour (Plenum, New York, 1988).
[2] *Annihilation in Gases and Galaxies*, edited by R. J. Drachman, NASA Conf. Publication No. 3058 (NASA, Greenbelt, MD, 1990).
[3] E. A. G. Armour, Comments At. Mol. Phys. **22**, 173 (1989).
[4] W. Raith and G. Sinapius, Comments At. Mol. Phys. **22**, 199 (1989).
[5] *Positron Annihilation Studies in Fluids*, edited by S. C. Sharma (World Scientific, Singapore, 1988).
[6] C. M. Surko, A. Passner, M. Leventhal, and F. J. Wysocki, Phys. Rev. Lett. **61**, 1831 (1988).
[7] E. A. G. Armour, Phys. Rep. **169**, 1 (1988).
[8] F. A. Gianturco and R. Melissa, Europhys. Lett. **33**, 661 (1996).
[9] F. A. Gianturco and T. Mukherjee, Phys. Rev. A **55**, 1044 (1997).
[10] F. A. Gianturco and T. Mukherjee, J. Phys. B (to be published).
[11] L. A. Collins and D. W. Norcross, Adv. At. Mol. Phys. **18**, 41 (1983).
[12] Y. Itikawa, Phys. Rep. **46**, 117 (1978).
[13] Ch. K. Kwan, Y. F. Hsieh, W. E. Kauppila, S. J. Smith, T. S. Stein, M. N. Uddin, and M. S. Dababneh, Phys. Rev. A **27**, 1328 (1983).
[14] O. Sueoka and S. Mori, J. Phys. Soc. Jpn. **53**, 2491 (1984).
[15] A. Jain, J. Phys. B **19**, L105 (1986).
[16] J. Tennyson and L. Morgan, J. Phys. B **20**, L641 (1987).
[17] A. Jain, J. Phys. B **238**, 863 (1990).
[18] A. Jain, Phys. Rev. A **41**, 2437 (1990).
[19] D. W. Norcross, Phys. Rev. A **25**, 764 (1982).
[20] F. A. Gianturco and A. Jain, Phys. Rep. **143**, 347 (1986).
[21] J. W. Darewych, J. Phys. B **15**, L415 (1982).
[22] B. K. Elza, T. L. Gibson, M. A. Morrison, and B. C. Saha, J. Phys. B **22**, 113 (1989).
[23] G. Danby and J. J. Tennyson, J. Phys. B **23**, 1005 (1990).
[24] J. O. O'Connel and N. F. Lane, Phys. Rev. A **27**, 1893 (1983).
[25] F. A. Gianturco, J. A. Rodriguez-Ruiz, and A. Jain, Phys. Rev. A **48**, 4321 (1993).
[26] J. A. Arponen and E. Pajanne, Ann. Phys. (N.Y.) **121**, 343 (1979).
[27] E. Boronski and R. M. Nieminen, Phys. Rev. B **34**, 3820 (1986).
[28] W. Kohn and L. J. Sham, Phys. Rev. **140**, A1133 (1965).
[29] M. A. Morrison, N. F. Lane, and L. A. Collins, Phys. Rev. A **15**, 2186 (1977).
[30] L. A. Collins and D. W. Norcross, Phys. Rev. A **18**, 478 (1978).
[31] D. W. Norcross and N. T. Padial, Phys. Rev. A **25**, 226 (1982).
[32] B. H. Choi and R. T. Poe, Phys. Rev. A **16**, 1821 (1977).
[33] M. A. Morrison, Adv. At. Mol. Phys. **29**, 123 (1988).
[34] For example, see N. F. Lane, Rev. Mod. Phys. **52**, 29 (1980).
[35] A. Temkin and K. V. Vasavada, Phys. Rev. A **169**, 190 (1967).
[36] P. McGuire and D. J. Kouri, J. Chem. Phys. **60**, 2488 (1974).
[37] F. A. Gianturco, N. Sanna, and S. Serna, J. Chem. Phys. **98**, 3833 (1993).
[38] A. D. McLean and M. Yoshimine, IBM J. Res. Dev. **12**, 206 (1967).
[39] N. Chandra and A. Temkin, Phys. Rev. A **13**, 188 (1976).
[40] W. Sohn, K.-H. Kochem, K. Jung, H. Ehrhardt, and E. S. Chang, J. Phys. B **18**, 2049 (1985).
[41] G. A. Gallup, J. Phys. B **23**, 2397S (1990).
[42] K.-H. Kochem, W. Sohn, K. Jung, H. Ehrhardt, and E. S. Chang, J. Phys. B **18**, 1253 (1985).
[43] K.-H. Kochem, W. Sohn, N. Hebel, K. Jung, and H. Ehrhardt, J. Phys. B **18**, 4455 (1985).
[44] N. Chandra, Phys. Rev. A **12**, 2342 (1975).
[45] A. M. Arthurs and A. Dalgarno, Proc. R. Soc. London, Ser. A **256**, 540 (1960).
[46] A. S. Gosh, T. Mukherjee, P. K. Biswas, and A. Jain, J. Phys. B **26**, L23 (1993).
[47] A. N. Feldt and M. A. Morrison, J. Phys. B **15**, 301 (1982).